ORIGINAL RESEARCH ARTICLE

Temperature-and Composition-Dependent Band Gap Energy and Electron–Phonon Coupling in InAs$_{1-x}$Sb$_x$ Semiconductors Alloys for Infrared Photodetection

Abderrazak Boutramine[1]

Abstract

This paper makes an improvement on the determination of the temperature, bowing parameter, and antimony (Sb) composition effects on the fundamental band gap energy of InAs$_{1-x}$Sb$_x$ ternary alloys for infrared (IR) photodetection. The present study was carried out in a broader temperature range from cryogenic to room temperature for the entire alloy range, and a reasonable analysis has also been carried out. Meanwhile, a proposed expression for the band gap bowing parameter temperature dependence has been established. The optical cut-off wavelength can be further tuned over a significant range up to 14 μm or more by altering the stoichiometry of InAs$_{1-x}$Sb$_x$ alloys. The three Varshni and Bose–Einstein thermodynamic parameters were found to exhibit a parabolic trend with Sb composition. Consequently, the quadratic equations relating these parameters to Sb composition were derived. The relatively weak band gap temperature coefficient reported here is hoped to offer an improvement on infrared photodetector (IR-PD) stability. Also, the average phonon energy and the corresponding electron–phonon coupling interaction strength were investigated versus Sb composition. The available experimental results were used, where possible, to confirm our theoretical estimates, and the agreement is satisfactory. We expect that the present work will be helpful in designing and improving the photodetection properties of IR optoelectronics devices. Additionally, it provides a firm basis for our forthcoming determination of the electronic band structure properties of InAs$_{1-x}$Sb$_x$ based superlattices.

Graphical Abstract
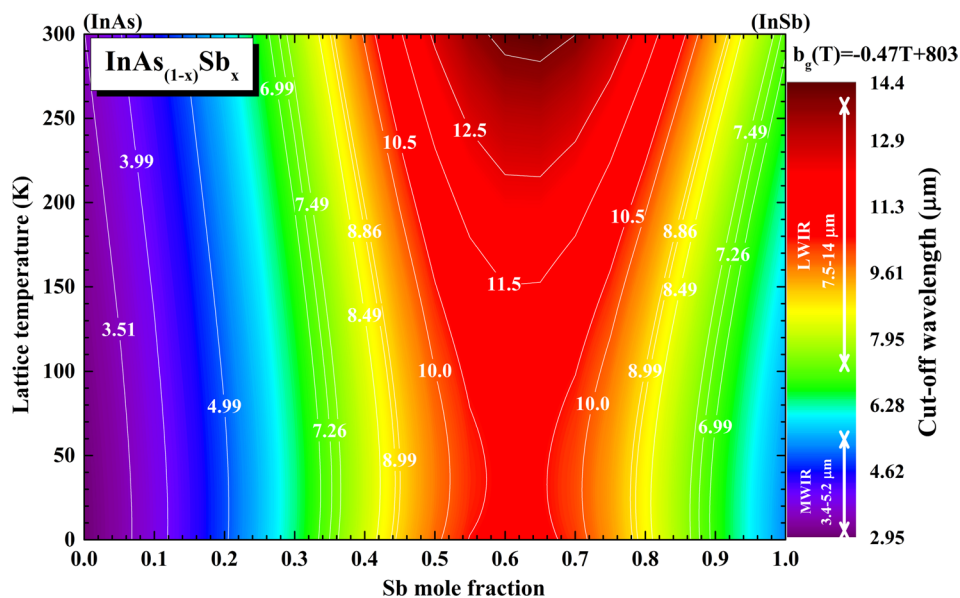
Extended author information available on the last page of the article

Introduction

Antimony (Sb)-containing ternary systems, such as InAs$_{1-x}$Sb$_x$, have garnered immense excitement and have been recognized as the material of choice for high-frequency optoelectronics devices. In particular, the fact that the magnitude of fundamental band gap energy can be tuned to absorb infrared (IR) radiation in the entire medium wavelength (MWIR: 3.4-5.2 μm), long wavelength (LWIR: 7.5-14 μm), and very long wavelength (VLWIR: > 14 μm) atmospheric transmission windows, makes this system almost perfect and ideal material in designing infrared photodetectors (IR-PDs).[1–3] Furthermore, due to its appealing features, including the weak ionic character[4] of its covalent bonding contribution, high optical quality, and good uniformity of epitaxial growth,[5] InAs$_{1-x}$Sb$_x$ provides a prevalent alternative candidate to their II–VI competitors, mainly Hg$_{1-x}$Cd$_x$Te (MCT) alloys, in terms of implementation in uncooled advanced IR-PDs.[6–9] Although MCT is a crucial material for MWIR and LWIR bands, there are still some challenges in terms of a lack of stability and non-uniformity over a large composition area due to the Hg vapor pressure. In addition, MCT-based IR-PDs work only under cryogenic conditions and are high-cost materials.

In practical design and simulation of InAs$_{1-x}$Sb$_x$ -based optoelectronics devices, a serious challenge lies in the control of optical cut-off wavelength, and hence its spectral response for a desired application. However, it is well known that the optical cut-off wavelength depends mainly on material composition and crystalline quality. Moreover, a high-quality semiconductor crystal is required to construct IR-PDs with excellent performances, and this often requires the PDs epitaxial layers to be grown with minimal defects and smooth interfaces, and be compositionally homogeneous. Despite the fact that several III–V substrates can be used for growing InAs$_{1-x}$Sb$_x$, the huge lattice mismatch leads to a poor crystal quality, drastically limiting the range of material composition. As a result, many properties of InAs$_{1-x}$Sb$_x$ alloys are still unknown due to the increased difficulties in growing high-quality materials and the decreased emission efficiency with increasing Sb composition. Hence, for device applications, improving the material quality and understanding the nonlinear optical properties of InAs$_{1-x}$Sb$_x$ in a wider composition range are greatly required.

In the recent past, there has been widespread interest toward the study of the temperature and compositional dependence of the electro-optical properties of InAs$_{1-x}$Sb$_x$ semiconductor alloys.[10–14] However, the observed significant spread among the reported data implies variations in the measured band gap energy of InAs$_{1-x}$Sb$_x$ alloys with the same composition, and reflects inaccuracies related to the difficulty in determining the actual material composition. Moreover, the difficulties in the synthesis of InAs$_{1-x}$Sb$_x$ semiconductor alloys and their structural and optical quality are strongly correlated with the mismatch between its parent elements directly reflected by the so-called bowing parameter. Hence, this parameter carries important information about the character of a given alloy and is most often compositionally independent. However, when the two binaries indium arsenide (InAs) and indium antimonide (InSb) are combined to form the InAs$_{1-x}$Sb$_x$ ternary alloy, the optical band gap energy versus x shows a distinct bowing behavior, rather than a linear relationship. Typically, it has been asserted that the deviation from a linear dependence, predicted by the virtual crystal approximation,[15] can be accounted for by including the effects of disorder on the conduction and valence band edges. Furthermore, in a more advanced treatment of this issue, it was assumed that the band gap bowing parameter can be routinely decomposed into three parts, originating from volume deformation, charge transfer effects, and structural relaxation.[16] Concurrently, it was also argued that a single bowing parameter can describe the band gap energy behavior in the whole composition range. In consequence, a large spread in the reported values of InAs$_{1-x}$Sb$_x$ band gap energy relies on accurate knowledge of the material band gap bowing parameter.

Moreover, after a comprehensive literature review, we have noticed a large spread in the reported values of InAs$_{1-x}$Sb$_x$ band gap bowing parameter.[17–21] The commonly accepted value is 670 meV, recommended by Vurgaftman et al.[22] However, no agreement has been reached on the magnitude of the band gap bowing parameter of InAs$_{1-x}$Sb$_x$ alloys, or even on the issue of whether a single bowing parameter can describe the band gap width over the entire composition range. It is also worth noting that the large reported values of the band gap bowing parameter are rather unusual for the band gap energies in regular semiconductor alloys such as InAs$_{1-x}$Sb$_x$. However, it has been clearly shown that the bowing parameter varies versus temperature in the range of b_g(low T) = 938 meV[17] to b_g(300 K) = 590 meV.[22] Meanwhile, the dependence of the bowing parameter on the composition in the aforementioned works is weak.

The purpose of this paper is to extend the theoretical description of the optical band gap energy and related parameters versus temperature in the whole Sb composition range ($0 \leq x \leq 1$). The results of this study provide several values of band gap-related parameters for $InAs_{1-x}Sb_x$, which should prove very useful for enable suitable applications, as well as for the correct determination of epitaxial growth conditions. Moreover, it is well known that the study of electronic transport and optical properties of semiconductor materials requires a sound knowledge of the non-negligible coupling between electrons and lattice phonons. Therefore, it is clearly of considerable value to provide information on the basic vibration properties in the alloys under investigation. The average phonon energy and the corresponding electron–phonon interaction strength were also investigated in a broader composition range.

Calculation Method

The first investigation of the nonlinearity behavior in the optical properties of the $InAs_{1-x}Sb_x$ alloys is indicated in the fundamental band gap energy, ε_g, compositional dependence, which can be modeled using a second-order polynomial relationship between the band gaps of two terminal binary compounds with a quadratic term proportional to the band gap bowing parameter:

$$\varepsilon_g^{InAsSb}(x, T) = x\varepsilon_g^{InSb}(1, T) + (1 - x)\varepsilon_g^{InAs}(0, T) - x(1 - x)b_g(T) \tag{1}$$

This relationship is valid not only for the fundamental band gap energy but also for other energy positions of the band structure with distinct bowing parameters. In this paper, our proposed band gap bowing parameter versus the lattice temperature is determined from:

$$b_g(T) = -0.47T + 803 \, (meV) \tag{2}$$

This equation has been benchmarked against experimental measurements, where we find that it can well reproduce the measured band gap energy versus Sb composition and temperature by introducing the temperature dependence of the InAs and InSb band gap energies. For the absorption layer, the relationship between the band gap energy of the material and its optical cut-off wavelength, λ_{cutoff}, is conventionally expressed as:

$$\lambda_{cutoff}(x, T) \times \varepsilon_g(x, T) = 1240 \, (\mu m \times meV) \tag{3}$$

The temperature effect on the fundamental band gap energy of $InAs_{1-x}Sb_x$ is important for device design, as most IR-PDs are cooled below room temperature to minimize the effects of irradiative recombination. Furthermore, it is well known that the total changes of the band gap energy in semiconductor materials under temperature follows from a shift in the relative positions of the conduction and valence bands due to the temperature dependence of (1) dilatation of the lattice, and (2) electron–phonon interaction, which forms the major contribution to the variation. In the present work, the effect of temperature on the fundamental band gap energy of $InAs_{1-x}Sb_x$ is described by using the Varshni[23] and Bose–Einstein[24] three-parameter thermodynamic models:

$$\varepsilon_g(T) = \varepsilon_{gv}(0) - \alpha_v\left(\frac{T^2}{\beta_v + T}\right) \tag{4}$$

$$\varepsilon_g(T) = \varepsilon_{gBE}(0) - \frac{2a_{BE}}{\left(e^{\frac{\theta_{BE}}{T}} - 1\right)} \tag{5}$$

where $\varepsilon_{gi}(0)$ (meV) is the 0 K band gap energy, α_v(meV/K) and $\beta_v(K)$ are material-dependent parameters, and T(K) is the temperature in Kelvin. The value of α_v(meV/K) is related to the thermal expansion of the lattice, and the value of $\beta_v(K)$ is thought to be similar to the Debye temperature, $\theta_D(K)$. Usually, above $\theta_D(K)$, the band gap energy changes almost linearly with temperature due to linear changes of the lattice parameters and electron–phonon interaction. The parameter $\theta_{BE}(K)$ describes the mean frequency of the phonons involved and a_{BE}(meV) describes the strength of the electron–phonon interaction. It is worth noting that the Bose–Einstein model retains physical meaning and enables an accurate extraction of average phonon energy, $< h\nu >$ (meV), for the material under investigation. However, these two models are related as follows:

$$\langle h\nu \rangle \approx k_B\theta_{BE} \approx 2k_B\beta_v \tag{6}$$

The band structure parameters of the two terminal binary compounds, InSb and InAs, have been investigated and refined over the years. A survey of the adopted values used in this study is summarized in Table I.

Table I Band structure parameters of InAs and InSb parents adopted in the present work, Λ is the valence band offset between the valence band maxima near the centre Γ of the first Brillouin zone of InAs and InSb

| Compound | Band structure parameters [22] | | | |
	$\varepsilon_{g(\Gamma-\Gamma)}$ (meV)	$\alpha_{v(\Gamma-\Gamma)}$ (meV/K)	$\beta_{v(\Gamma-\Gamma)}$ (K)	Λ (meV)
InAs	417	0.276	93	−590 [25]
InSb	235	0.320	170	

Results and Discussion

The $InAs_{1-x}Sb_x$ cut-off wavelength versus Sb composition is depicted in Fig. 1 for both low (Fig. 1a) and room (Fig. 1b) temperatures. The continuous and short dashed lines are the calculated results obtained using our band gap bowing parameter given by Eq. (2) and that adopted by Murawski el al.,[26] respectively. Also shown for comparison are the available experimental data reported in the literature. As presented in Fig. 1, the cut-off wavelengths of $InAs_{1-x}Sb_x$ under investigation vary rapidly at the dilute Sb composition side, but changes slowly at the relatively large Sb composition side. A close inspection of Fig. 1 demonstrates that the incorporation of dilute Sb composition into the InAs host material has been shown to enhance the cut-off wavelength by a linearized average rate of about 1.90 μm, and by 1.41 μm per 10% Sb content at room and low temperatures, respectively. This rapid increase of cut-off wavelengths, with the bowing parameter spanning the range of 662–801 meV, implies that the Sb incorporation significantly perturbs the band structure of the InAs pristine compound. Also, Fig. 1 shows the existence of $InAs_{1-x}Sb_x$ alloys capable of reaching the LWIR regime with relatively lower bowing values than previously reported. Interestingly, reaching the beginning

of the LWIR regime at approximately 7.5 μm needs a bowing parameter of 662 meV for only 25% Sb content and 801 meV for 35% Sb content at room and liquid helium temperatures, respectively.

The proper correlation between our theoretical results and the available experimental ones was reached for both As-rich ($x < 0.5$) and Sb-rich ($x > 0.5$) sides. In a moderate composition range, especially at room temperature, no such credible data are available. Furthermore, in the low-temperature range, our results deviate from the photoluminescence predictions substantially in the range of 0.40–0.65 Sb content. Additionally, the data determined from the optical transmission measurements, for samples grown by the metal organic chemical vapor deposition technique on lattice mismatched GaAs substrates, fits well with our bowing parameter at the Sb-rich side. It is believed that the relatively higher cut-off wavelengths (lower band gap energies) observed in the experimental reported values were masked partly by electron filling of the conduction band due to background doping, as these samples were grown with various degrees of residual strain and relaxation. Consequently, the slight deviation of our data from the experimental ones can be attributed to the copper–platinum (CuPt)-type atomic ordering of the material, hypothesized to be caused mainly by residual strain.

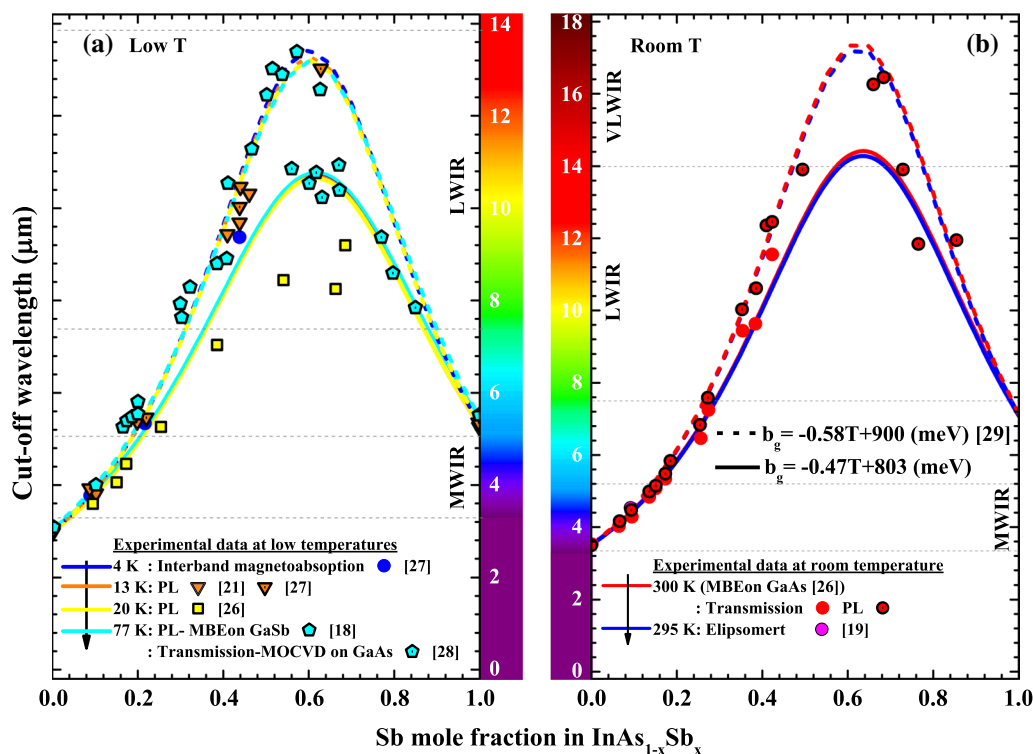The size and core electronic structure of Sb ($Z = 51$, $R_{atom} = 140$ pm) are significantly different from those of As

Fig. 1 $InAs_{1-x}Sb_x$ optical cut-off wavelengths versus the Sb composition at (a) low temperature and (b) room temperature. The available experimental data were taken from selected works as indicated by the legend. *MBE* molecular beam epitaxy technique.

($Z = 33$, $R_{atom} = 120$ pm). As expected, the substitution of As by Sb implies an average increase in the unit cell volume. Thus, a compressive strain develops in the crystal resulting in a significant modification in the electronic structure and related electro-optical properties of the pristine alloys. Furthermore, the different behaviors of the cut-off wavelengths observed on both the As- and Sb-rich sides suggest different origins of the band gap bowing which could be explained as follows (Fig. 2). First, as depicted in Fig. 2a for the As-rich side, incorporating a small amount of Sb into the InAs can introduce a localized Sb-level lying below the valence band maximum (ΓVBM) of InAs near the first Brillouin zone Γ center. This induced localized Sb-level has a strong effect on the ΓVBM of the InAs host material. Consequently, the coupling interaction between them can lead to the upward movement of the ΓVBM of InAs$_{1-x}$Sb$_x$, thus enhancing the cut-off wavelengths when the Sb content is relatively high. Second, Fig. 2b clearly shows that, at the Sb-rich side, an increasing trend of the cut-off wavelengths with increasing As content can be observed. The reason is because a localized As level can be introduced after incorporating a small amount of As into the InSb host material. This localized As level is located above the Γ conduction band minimum (ΓCBm) of the InSb. When the As content increases, the coupling interaction strength between the As level and the ΓCBm of

the InSb is enhanced. Furthermore, this enhanced coupling interaction strength is able to push down the ΓCBm of the InAs$_{1-x}$Sb$_x$, leading to the cut-off wavelengths increase in the Sb-rich range.

To further validate the obtained values, Fig. 3 depicts that the satisfactory agreement between our calculation and the experiment, over the entire composition range, shows
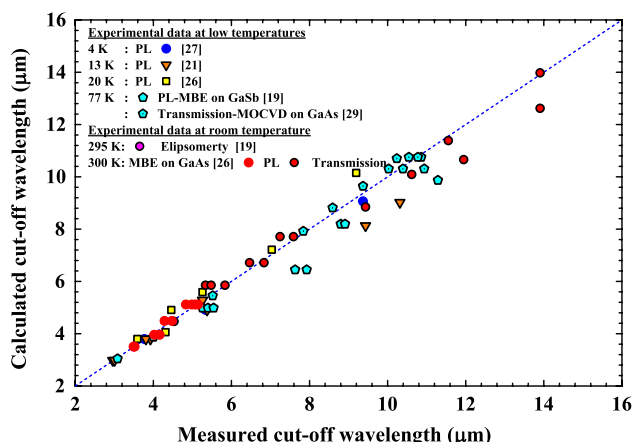
Fig. 3 Calculated versus the available measured InAs$_{1-x}$Sb$_x$ cut-off wavelengths in the entire Sb composition range.
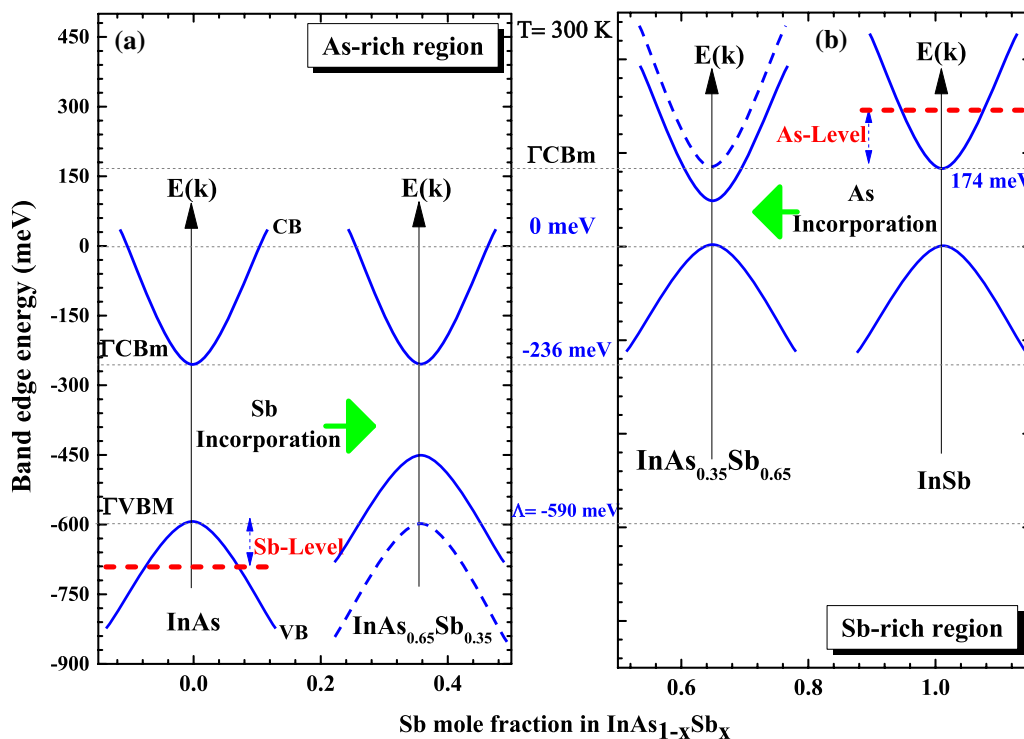
Fig. 2 Schematic showing the Sb composition dependence of energy positions of the conduction band minimum (ΓCBm) and valence band maximum (ΓVBM) band edges for InAs$_{1-x}$Sb$_x$. The ΓVBM was chosen as $\Lambda = -590$ meV for InAs and 0 meV for InSb. (a) The InAs band structure and the effect of the localized Sb level in the InAs$_{0.65}$Sb$_{0.35}$ As-rich alloy. (b) The conduction band edge InSb host material shift below As level in the InAs$_{0.35}$Sb$_{0.65}$ Sb-rich alloy.

confidence in the measuring procedures used in the selected works, as well as the success of our data analysis method, and offers assurance for investigating other effects due to Sb incorporation. Although, among other effects, some tensile strain is believed to exist in the $InAs_{1-x}Sb_x$ epitaxial reference samples, their band gap energies and the corresponding cut-off wavelength values are either in agreement or only slightly below the results reported in this study. Furthermore, Fig. 3 clearly shows that some measured values are found to be larger than the corresponding theoretically predicted ones. This may be attributed to errors in experimental measurements and/or the dominance of the disordered excited states in the samples. Meanwhile, it is worth noting that, for a given concentration, the band gap energy of the ground states is generally larger than the excited states energy.

It is plausible to investigate the complete optical cut-off wavelength temperature dependence in the entire Sb composition range. However, due to the relatively large band gap energies, a wide range of temperature is very much needed for an accurate description of the temperature effect. As seen from Fig. 4, for a fixed composition value, the cut-off wavelength followed an increasing trend in quite similar ways with increasing the sample temperature. Moreover, in the As-rich side, the enhanced cut-off wavelength with Sb content is roughly 3.51 μm in the MWIR band for pure InAs and 8.86 μm in the LWIR band for $InAs_{0.65}Sb_{0.35}$ at room temperature. Simultaneously, at liquid helium temperature, the cut-off wavelength decreases to 2.97 μm for pure InAs and to 7.26 μm for $InAs_{0.65}Sb_{0.35}$, enabling it to cover both MWIR

and LWIR atmospheric windows. The total cut-off wavelength red shift follows from the lowering in the band gap energy variation from 63.16 meV in InAs to only 30.86 meV in $InAs_{0.65}Sb_{0.35}$ as the temperature increases.

The present findings confirm that the two conventional $InAs_{0.40}Sb_{0.60}$ and $InAs_{0.35}Sb_{0.65}$ samples exhibit sufficiently high possible cut-off wavelengths implying longer absorption in the LWIR and VLWIR atmospheric windows. Furthermore, Fig. 5 clearly indicates that the longest cut-off wavelengths that can be quenched by the 662-meV bowing
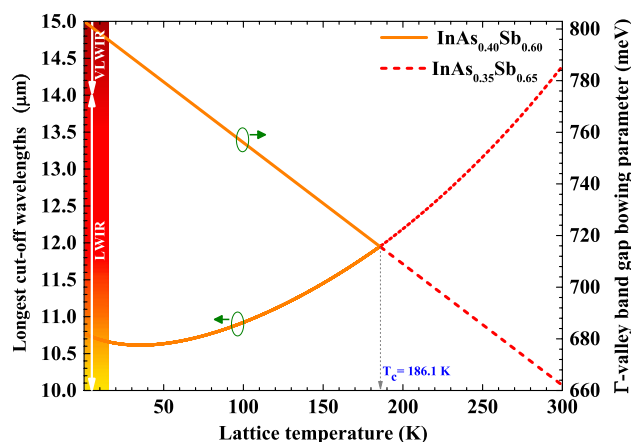

Fig. 5 Longest cut-off wavelengths and the corresponding band gap bowing parameter as a function of lattice temperature for $InAs_{0.40}Sb_{0.60}$ (solid curve for $T < T_c = 186.1$ K) and $InAs_{0.35}Sb_{0.65}$ (dashed curve for temperatures greater than $T_c = 186.1$ K).
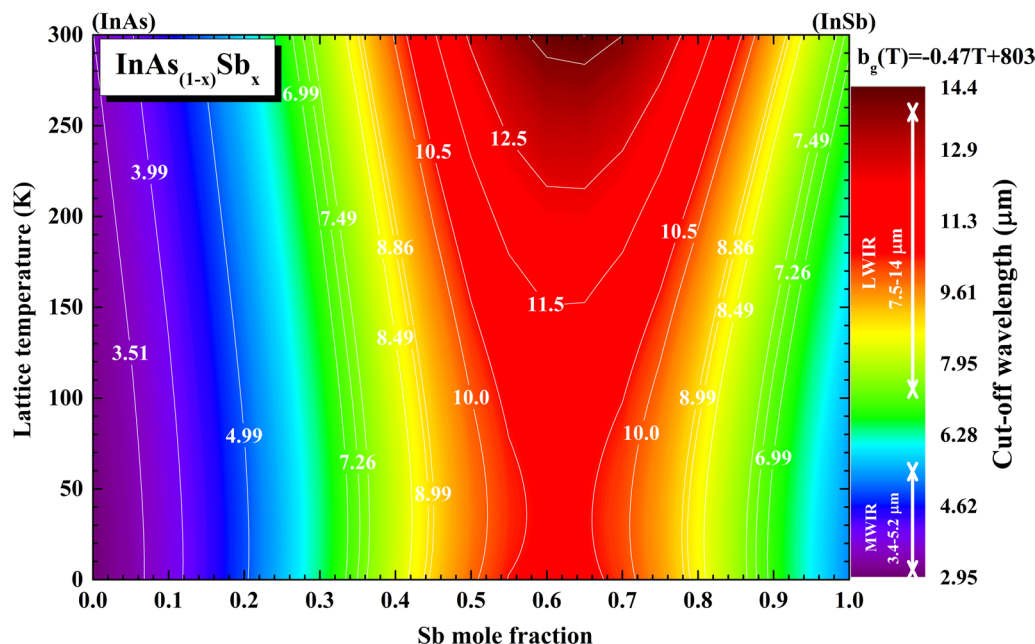

Fig. 4 Simulated contour maps of the dependence of the optical cut-off wavelength on both Sb composition and lattice temperature in the $InAs_{1-x}Sb_x$ alloy system. The calculations were carried out using our proposed band gap bowing parameter temperature dependence.

parameter is about 14.40 μm in the VLWIR atmospheric windows at room temperature and approximately 10.73 μm in the LWIR atmospheric band with 801 meV at liquid helium temperature. In consequence, the longest cut-off wavelength values also decline formidably when the lattice temperature decreases. The corresponding total red shift is about 1.20 μm in InAs$_{0.40}$Sb$_{0.60}$ for $T < T_c$ and 2.43 μm for InAs$_{0.35}$Sb$_{0.65}$ beyond $T_c = 186.1$ K.

The compositional dependence of the Varshni parameters, $\alpha_v (meV/K)$ and $\beta_v(K)$, for InAs$_{1-x}$Sb$_x$, is difficult to determine because of the observed scatter in the available data. Furthermore, the alloy composition was limited to a narrow region. The $\alpha_v(meV/K)$ and $\beta_v(K)$ parameters determined previously for the InAs$_{1-x}$Sb$_x$ samples are listed in Table III. The observed discrepancy in the corresponding values is probably from sample-dependent features such as strain and defects. Also, this is presumably caused by the difference in the incorporation scheme of Sb atoms into InAs$_{1-x}$Sb$_x$ and relevant localized states at a microscopic scale.

The temperature-induced band gap energy red shift for InAs$_{0.65}$Sb$_{0.35}$ and InAs$_{0.35}$Sb$_{0.65}$ together with that of InAs and InSb are depicted in Fig. 6. Based on the Varshni model, the total red shift of the band gap energies between 4 K and 300 K are 63.16 meV, 30.84 meV, 30.27 meV, and 61.25 meV for $x = 0$, 0.35, 0.65, and 1, respectively. Accordingly, with increasing Sb content, the optical band gap energy is less sensitive to the temperature changes. Such a functional dependence of the optical band gap energy on Sb composition can be commonly given in terms of the Varshni and Bose–Einstein parameters. Fitting $\varepsilon_g(T)$ in the entire composition range, using the Levenberg–Marquardt method, expresses the nonlinearity composition dependence of the Varshni and Bose–Einstein coefficients with the following general equation:

$$P_{InAsSb}(x, T) = xP_{InSb} + (1 - x)P_{InAs} - x(1 - x)b_i \qquad (7)$$

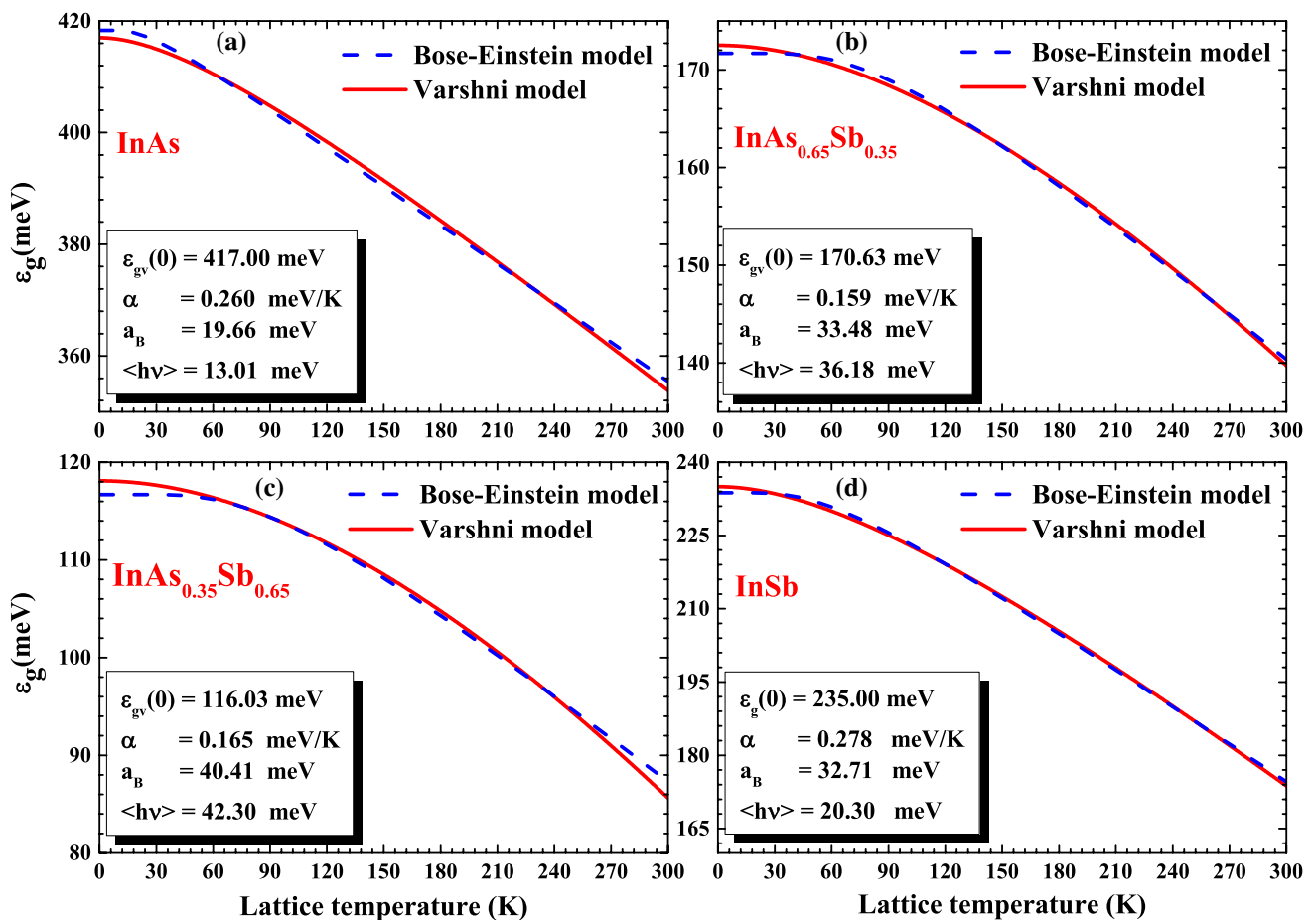**Fig. 6** Fundamental band gap energies as a function of lattice temperature for InAs$_{0.65}$Sb$_{0.35}$ and InAs$_{0.35}$Sb$_{0.65}$ ternary alloys together with that of InAs and InSb. The *solid* and *dashed curves* correspond to the Varshni and Bose–Einstein models, respectively. A list of the extracted fitting parameters using the Levenberg–Marquardt method are shown for each case.

The bowing parameter values b_i offering the best fits are listed in Table II.

Figure 7 shows that the 0-K band gap energy of InAs is 182 meV higher than that of InSb. One can see that the incorporation of Sb composition from 0 to 0.6 in the InAs host material causes a 0-K band gap energy red shift with a linearized average rate of 5 meV per 1% Sb content. Furthermore, the 0-K band gap energy minimum occurs for $InAs_{0.40}Sb_{0.60}$ implying longer absorption cut-off wavelengths. Interestingly, the temperature coefficient, α_v(meV/K), of the $InAs_{1-x}Sb_x$ alloys is appreciably smaller compared with that of the InSb. This is reflected by a shift by approximately 57% in $InAs_{0.40}Sb_{0.60}$ compared with that

of InSb. This result is hoped to offer an improvement on $InAs_{1-x}Sb_x$ optoelectronics-based device stability. However, no clear explanation of the observed effects has yet been offered. Additionally, for $x < 0.6$, the band gap temperature coefficient of $InAs_{1-x}Sb_x$ lies in a narrow range of 0.260–0.158 meV/K. It appears that, in this composition region, the band gap energy is less sensitive to the temperature and that incorporating 60% Sb has a relatively little effect on the temperature dependence of the band gap energy. These results illustrate a promising feature of the Sb-containing III–V alloys for the temperature-insensitive semiconductor materials for optoelectronic devices.

The average phonon energy $<h\nu>$ (meV) and the corresponding electron–phonon interaction strength, a_{BE} (meV), as a function of Sb composition are depicted in Fig. 7c, d, as well as the corresponding upper and lower confidence limits curves. One can see that $<h\nu>$ and a_{BE} versus x are found to exhibit a strong correlation with a negative bowing parameter, as listed in Table II. Additionally, the average phonon energy in the pseudo-binary $InAs_{0.10}Sb_{0.90}$ alloy is comparable to the thermal energy at room temperature, and the electron–phonon interaction

Table II Calculated bowing parameters values for the three Varshni and Bose–Einstein parameters

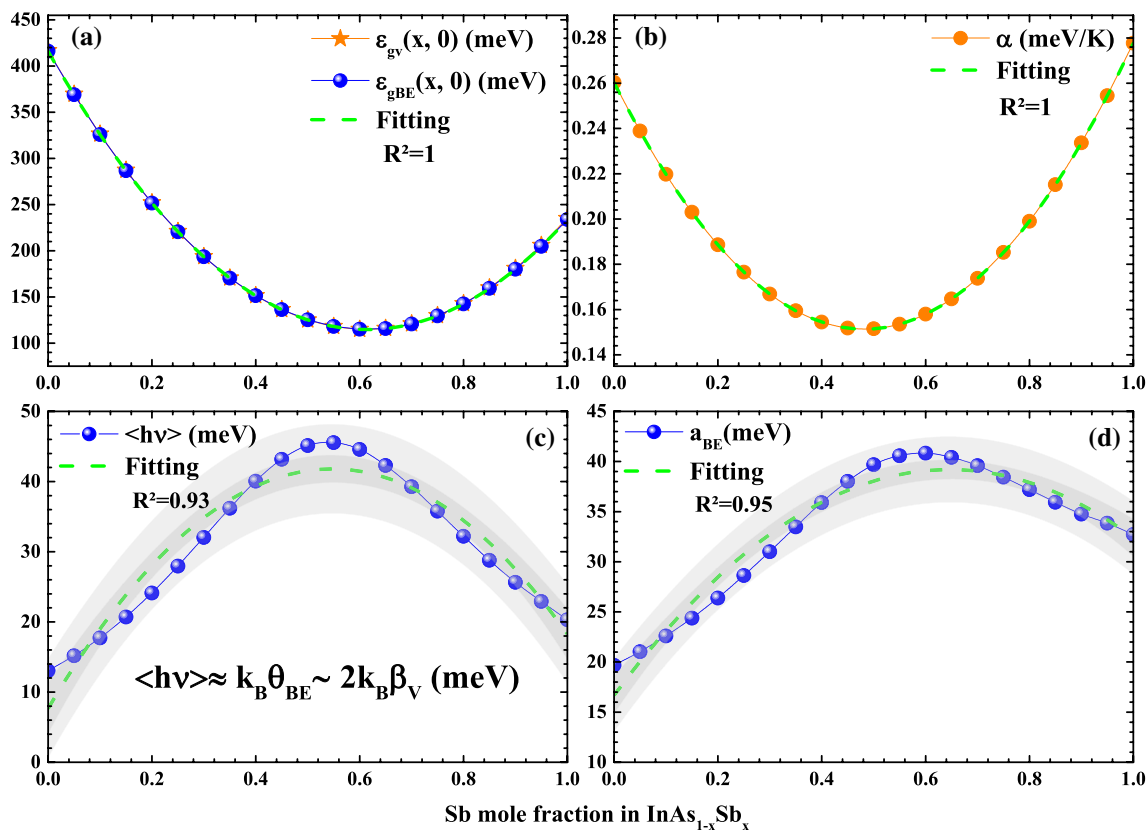| Varshni model			Bose–Einstein model		
b_{gv}(meV)	$b_{\alpha v}$ (meV/K)	$b_{\beta v}$(K)	b_{gBE}(meV)	$b_{\Theta BE}$(K)	b_{aBE}(meV)
802.95	0.47	−667.78	799.26	−1112.82	−45.80

Fig. 7 Compositional dependence of the (a) fundamental 0-K band gap energies for the two models adopted here, (b) band gap temperature coefficient, (c) average phonon energy, and (d) the corresponding strength of electron–phonon interaction in $InAs_{1-x}Sb_x$; the hashed gray area represents the corresponding upper–lower confidence limits, and the solid green lines are fitted curves drawn using the Levenberg–Marquardt method (Color figure online).

Table III Comparison of the three Varshni and Bose–Einstein parameters with the available results for similar compositions in $InAs_{1-x}Sb_x$ ternary alloys

Varshni model		$\varepsilon_{gv}(0)$ (meV)		α_v (meV/K)		β_v (K)	
Compound	x_{Sb}	This work	Expt.	This work	Expt.	This work	Expt.
InAs	0.00	417.00	417 [22]	0.260	0.276 [22]	75.75	93 [22]
	0.10	326.53	330 [19]	0.220	0.256 [19]	103.20	128 [19]
	0.20	252.13	226 [25]	0.188	0.320 [25]	140.47	100 [25]
	0.44	136.37	119 [25]	0.151	0.120 [25]	251.70	–
InSb	1.00	235.00	235 [22]	0.278	0.320 [22]	118.40	170 [22]
Average deviation		5.44%		20.01%		27.19%	
Bose–Einstein model		$\varepsilon_{gBE}(0)$ (meV)		$<h\nu>$ (meV)		a_{BE} (meV)	
Compound	x_{Sb}	This work	Expt.	This work	Expt.	This work	Expt.
InAs	0.00	416.23	417 [22]	13.01	13.00 [29]	19.66	22.00 [29]
	0.10	325.88	325 [19]	17.72	21.00 [19]	22.60	30.50 [19]
	0.95	204.74	214 [30]	22.92	36.00 [30]	33.83	–
InSb	1.00	233.82	235 [22]	20.30	12.50 [31]	32.71	18.80 [31]
Average deviation		1.32%		28.61%		36.84%	

is significantly strong. Moreover, the Varshni parameters determined for $InAs_{1-x}Sb_x$ alloys lie in between values of those parameters for InAs and InSb. Concurrently, the average phonon energy and the corresponding strength of electron–phonon interaction in $InAs_{1-x}Sb_x$ are higher than that of InAs and InSb.

Table III summarizes the presently obtained Varshni and Bose–Einstein parameters for $InAs_{1-x}Sb_x$ together with the previously available values for similar compositions. To further validate our obtained values for $InAs_{1-x}Sb_x$ ternary alloys, the direct comparison can be made for InAs and InSb binary compounds because the effects due to compositional fluctuation are absent. Obviously, satisfactory agreement between the present values and the corresponding experimental data is observed with a relatively slight average deviation. These results make us conclude that the irregular changes in the reported values may be sample-dependent, in the sense that they may be related to imperfections in the samples, such as, impurities, built-in strain, stress, or defects. Moreover, for the Varshni parameters, the rather different values of α_v (meV/K) and β_v (K) listed in Table III lead to almost identical band gap energy results over a significant temperature range. In addition, a reliable determination of band gap energy versus temperature can be obtained with a suitable combination of α_v (meV/K) and β_v (K).

Our results regarding $\varepsilon_g(0)$ and (α/β) for $InAs_{1-x}Sb_x$ are shown in Fig. 8. Also shown for comparison are the available data obtained exploiting the $\varepsilon_g(T, x)$ relationship reported in Ref. 32. Apparently, our predicted results overlap the results of Ref. 32 over a significant composition range.

The deviation of our value of (α/β) from the experimental ones is less than 39% for $x < 0.1$.

Conclusions

Despite the progress in current research on the electro-optical properties of the $InAs_{1-x}Sb_x$ alloy system, uncertainties remain regarding the fundamental basis of their band structure-related properties, ultimately rooted in its temperature and compositional dependence. Moreover, for an effective design and simulation of $InAs_{1-x}Sb_x$-based infrared photodetectors, as well as the correct determination of epitaxial growth conditions, it is clearly of considerable value to investigate the band gap energy dependence on temperature and composition over a significant range. In this work, we have reported on the dependence of the fundamental band gap energy of $InAs_{1-x}Sb_x$, and the corresponding cut-off wavelength, on temperature with Sb compositions spanning the entire range. The results reveal entirely different origins of the high cut-off wavelength bowing for the Sb-rich and As-rich sides. The relatively weaker band gap temperature coefficients reported in this work clearly illustrate promising features of Sb-containing alloy systems for the temperature-insensitive semiconductor materials optimized for infrared technology. Also, a correlation between the average phonon energy and the corresponding electron–phonon coupling interaction strength were observed over the entire Sb composition range. The reported results are likely to serve as a useful reference for improving the photodetection parameters
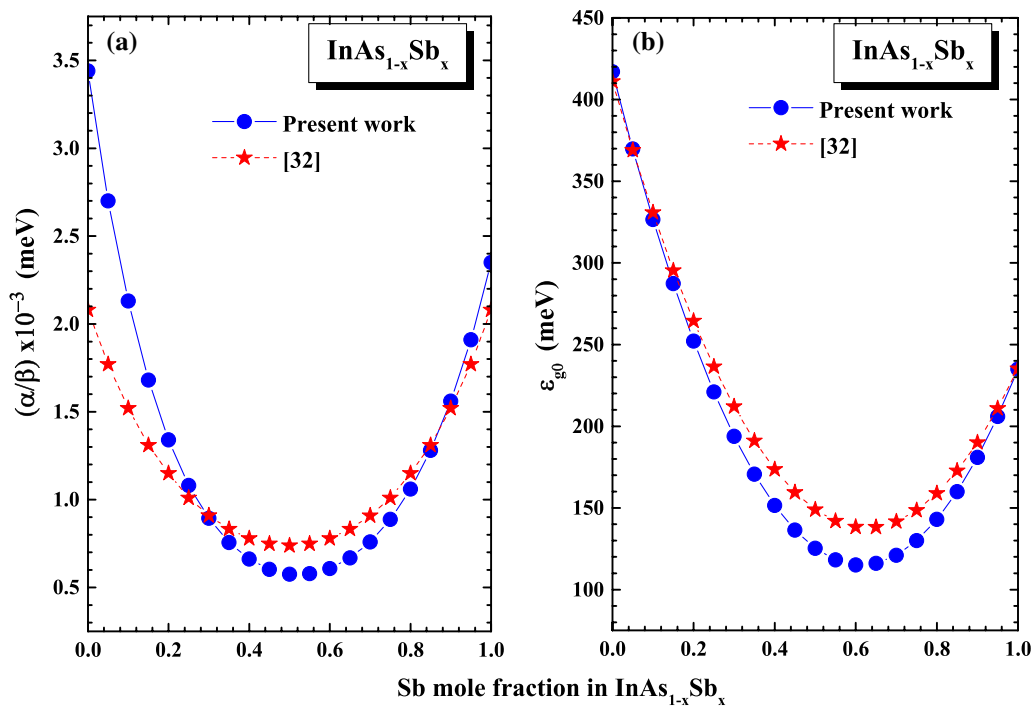
Fig. 8 Comparison of the composition dependence of (a) α/β and (b) 0-K fundamental band gap energy of InAs$_{1-x}$Sb$_x$.

of InAs$_{1-x}$Sb$_x$ -based devices, not only by improving the material quality, through a precise determination of epitaxial growth conditions, but also by very accurate designing of their structures. The satisfactory agreement with the available results yields confidence in our estimating procedure as well as our data analysis.

References

1. K. Michalczewski, D. Benyahia, J. Jureńczyk, D. Stępień, A. Kębłowski, J. Boguski, J. Rutkowski, and J. Piotrowski, High operating temperature LWIR and VLWIR InAs$_{1-x}$Sb$_x$ optically immersed photodetectors grown on GaAs substrates. *Infrared Phys. Technol.* 97, 116 (2019).
2. M.R. Biefeld, The metal-organic chemical vapor deposition and properties of III–V antimony-based semiconductor materials. *Mater. Sci. Eng. R Rep.* 36, 105 (2002).
3. W. Dobbelaere, J. De Boeck, C. Bruynserede, R. Mertens, and G. Borghs, Electron, InAsSb light emitting diodes and their applications to infrared gas sensors. *Electron. Lett.* 10, 890 (1993).
4. S. Adachi, *Properties of semiconductor alloys: group-IV, III-V and II-VI semiconductors*, 1st ed., (Wiley: New Jersey, 2009).
5. S.V. Ivanov, A.N. Semenov, V.A. Solovev, O.G. Lyublinskaya, Y.V. Terentev, B.. Ya.. Meltser, L.G. Prokopova, A.A. Sitnikova, A.A. Usikova, A.A. Toropov, and P.S. Kopev, Molecular beam epitaxy of type II InSb/InAs nanostructures with InSb sub-monolayers. *J. Cryst. Growth.* 278, 72 (2005).
6. H. Xie, H. Lin, Z. Zhou, Z. Wen, Y. Sun, J. Hao, S. Hu, and N. Dai, Room-temperature InAsSb pBin detectors for mid-infrared application. *Infrared Phys. Technol.* 128, 104475 (2023).
7. H.J. Lee, S.Y. Ko, Y.H. Kim, and J. Nah, Surface leakage current reduction of InAsSb nBn MWIR HOT detector via hydrogen peroxide treatment. *Infrared Phys. Technol.* 112, 103597 (2021).
8. G. Deng, W. Yang, X. Gong, and Y. Zhang, High-performance uncooled InAsSb-based pCBn mid-infrared photodetectors. *Infrared Phys. Technol.* 105, 103260 (2020).
9. D. Benyahia, K. Michalczewski, A. Kębłowski, P. Martyniuk, J. Piotrowski, and A. Rogalski, Investigation on the InAs$_{1-x}$Sb$_x$ epilayers growth on GaAs (001) substrate by molecular beam epitaxy. *J. Semicond.* 39, 033003 (2018).
10. D. Wang, D. Donetsky, G. Kipshidze, Y. Lin, L. Shterengas, G. Belenky, W. Sarney, and S. Svensson, Metamorphic InAsSb-based barrier photodetectors for the long wave infrared region. *Appl. Phys. Lett.* 103, 051120 (2013).
11. G. Belenky, G. Kipshidze, D. Donetsky, S.P. Svensson, W.L. Sarney, H. Hier, L. Shterengas, D. Wang, and Y. Lin, Effects of carrier concentration and phonon energy on carrier lifetime in type-2 SLS and properties of InAs$_{1-x}$Sb$_x$ alloys. *Infrared Technol. Appl.* XXXVII, 318 (2011).

12. G. Belenky, D. Donetsky, G. Kipshidze, D. Wang, L. Shterengas, W.L. Sarney, and S.P. Svensson, Properties of unrelaxed $InAs_{1-x}Sb_x$ alloys grown on compositionally graded buffers. *Appl. Phys. Lett.* 99, 141116 (2011).

13. V.K. Dixit, B. Bansal, V. Venkataraman, H.L. Bhat, and G.N. Subbanna, Structural, optical, and electrical properties of bulk single crystals of $InAs_xSb_{1-x}$ grown by rotatory Bridgman method. *Appl. Phys. Lett.* 81, 1630 (2002).

14. J.C. Woolley, and J. Warner, Optical energy-gap variation in InAs–InSb alloys. *Can. J. Phys.* 42, 1879 (1964).

15. N.J. Ramer, and A.M. Rappe, Virtual-crystal approximation that works: locating a compositional phase boundary in $Pb(Zr_{1-x}Ti_x)O_3$. *Phys. Rev. B.* 62, R743 (2000).

16. J.E. Bernard, and A. Zunger, Electronic structure of ZnS, ZnSe, ZnTe, and their pseudobinary alloys. *Phys. Rev. B.* 36, 3199 (1987).

17. S. Tomasuloa, C.A. Affouda, N.A. Mahadik, M.E. Twigg, M.K. Yakes, and E.H. Aifer, Sb-incorporation in MBE-grown metamorphic InAsSb for long-wavelength infrared applications. *J. Vac. Sci. Technol.* 36, 02D108 (2018).

18. Y. Lin, D. Donetsky, D. Wang, D. Westerfeld, G. Kipshidze, L. Shterengas, W.L. Sarney, S.P. Svensson, and G. Belenky, Development of bulk InAsSb alloys and barrier heterostructures for long-wave infrared detectors. *J. Electron. Mater.* 44, 3360 (2015).

19. P.T. Webster, N.A. Riordan, S. Liu, E.H. Steenbergen, R.A. Synowicki, Y.-H. Zhang, and S.R. Johnson, Measurement of InAsSb bandgap energy and InAs/InAsSb band edge positions using spectroscopic ellipsometry and photoluminescence spectroscopy. *J. Appl. Phys.* 118, 245706 (2015).

20. P.T. Webster, N.A. Riordan, S. Liu, E.H. Steenbergen, R.A. Synowicki, Y.-H. Zhang, and S.R. Johnson, Absorption properties of type-II InAs/InAsSb superlattices measured by spectroscopic ellipsometry. *Appl. Phys. Lett.* 06, 061907 (2015).

21. S.P. Svensson, W.L. Sarney, H. Hier, Y. Lin, D. Wang, D. Donetsky, L. Shterengas, G. Kipshidze, and G. Belenky, Band gap of $InAs_{1-x}Sb_x$ with native lattice constant. *Phys. Rev. B.* 86, 245205 (2012).

22. I. Vurgaftman, J. Meyer, and L.R. Ram-Mohan, Band parameters for III–V compound semiconductors and their alloys. *J. Appl. Phys.* 89, 5815 (2001).

23. Y.P. Varshni, Temperature dependence of the energy gap in semiconductors. *Physica.* 34, 149 (1967).

24. R. Pässler, Semi-empirical descriptions of temperature dependences of band gaps in semiconductors. *Phys. Status Solidi C.* 236, 710 (2003).

25. Y. Lin, D. Wang, D. Donetsky, L. Shterengas, G. Kipshidze, G. Belenky, S.P. Svensson, W.L. Sarney, and H.S. Hier, Conduction-and valence-band energies in bulk $InAs_{1-x}Sb_x$ and type II $InAs_{1-x}Sb_x$/InAs strained-layer superlattices. *J. Electron. Mater.* 42, 918 (2013).

26. K. Murawski, E. Gomółka, M. Kopytko, K. Grodecki, K. Michalczewski, Ł Kubiszyn, W. Gawron, P. Martyniuk, A. Rogalski, and J. Piotrowski, Band gap energy determination of InAsSb epilayers grown by molecular beam epitaxy on GaAs substrates. *Prog. Natl. Sci. Mater. Int.* 29, 472 (2019).

27. S. Suchalkin, J. Ludwig, G. Belenky, B. Laikhtman, G. Kipshidze, Y. Lin, and L. Shterengas, Electronic properties of unstrained unrelaxed narrow gap $InAs_xSb_{1-x}$ alloys. *J. Phys. D Appl. Phys.* 49, 105101 (2016).

28. J.D. Kim, D. Wu, J. Wojkowski, J. Piotrowski, J. Xu, and M. Razeghi, Long-wavelength InAsSb photoconductors operated at near room temperatures (200–300 K). *Appl. Phys. Lett.* 68, 99 (1996).

29. I.A. Vainshtein, A.F. Zatsepin, and V.S. Kortov, Applicability of the empirical Varshni relation for the temperature dependence of the width of the band gap. *Phys. Solid State* 41, 905 (1999).

30. B. Bhavtosh, V.K. Dixit, V. Venkataraman, and H.L. Bhat, Temperature dependence of the energy gap and free carrier absorption in bulk $InAs_{0.05}Sb_{0.95}$ single crystals. *Appl. Phys. Lett.* 82, 4720 (2003).

31. Z.M. Fang, K.Y. Ma, D.H. Jaw, R.M. Cohen, and G.B. Stringfellow, Photoluminescence of InSb, InAs, and InAsSb grown by organometallic vapor phase epitaxy. *J. Appl. Phys.* 67, 7034 (1990).

32. H.H. Wieder, and A.R. Clawson, Photoelectronic properties of $InAs_{0.07}Sb_{0.93}$ films. *Thin Solid Films.* 15, 217 (1973).

Authors and Affiliations

Abderrazak Boutramine[1]

✉ Abderrazak Boutramine
  Abderrazak.boutramine@gmail.com

1 Ibn Zohr University, 80000 Agadir, Morocco